

# High-resolution Photo-excitation Measurements Exacerbate the Long-standing Fe XVII-Emission Problem

Steffen Kühn,<sup>1,2,\*</sup> Chintan Shah,<sup>1,3,†</sup> José R. Crespo López-Urrutia,<sup>1</sup> Keisuke Fujii,<sup>4</sup> René Steinbrügge,<sup>5</sup> Jakob Stierhof,<sup>6</sup> Moto Togawa,<sup>1</sup> Zoltán Harman,<sup>1</sup> Natalia S. Oreshkina,<sup>1</sup> Charles Cheung,<sup>7</sup> Mikhail G. Kozlov,<sup>8,9</sup> Sergey G. Porsev,<sup>8,7</sup> Marianna S. Safranova,<sup>7,10</sup> Julian C. Berengut,<sup>11,1</sup> Michael Rosner,<sup>1</sup> Matthias Bissinger,<sup>12,6</sup> Ralf Ballhausen,<sup>6</sup> Natalie Hell,<sup>13</sup> SungNam Park,<sup>14</sup> Moses Chung,<sup>14</sup> Moritz Hoesch,<sup>5</sup> Jörn Seltmann,<sup>5</sup> Andrey S. Surzhykov,<sup>15,16</sup> Vladimir A. Yerokhin,<sup>17</sup> Jörn Wilms,<sup>6</sup> F. Scott Porter,<sup>3</sup> Thomas Stöhlker,<sup>18,19,20</sup> Christoph H. Keitel,<sup>1</sup> Thomas Pfeifer,<sup>1</sup> Gregory V. Brown,<sup>13</sup> Maurice A. Leutenegger,<sup>3</sup> and Sven Bernitt<sup>1,18,19,20</sup>

<sup>1</sup>Max-Planck-Institut für Kernphysik, Saupfercheckweg 1, 69117 Heidelberg, Germany

<sup>2</sup>Heidelberg Graduate School of Fundamental Physics, Ruprecht-Karls-Universität Heidelberg, Im Neuenheimer Feld 226, 69120 Heidelberg, Germany

<sup>3</sup>NASA/Goddard Space Flight Center, 8800 Greenbelt Rd, Greenbelt, MD 20771, USA

<sup>4</sup>Department of Mechanical Engineering and Science, Graduate School of Engineering, Kyoto University, Kyoto 615-8540, Japan

<sup>5</sup>Deutsches Elektronen-Synchrotron DESY, Notkestraße 85, 22607 Hamburg, Germany

<sup>6</sup>Dr. Karl Remeis-Sternwarte, Sternwartstraße 7, 96049 Bamberg, Germany

<sup>7</sup>Department of Physics and Astronomy, University of Delaware, Newark, Delaware 19716, USA

<sup>8</sup>Petersburg Nuclear Physics Institute of NRC "Kurchatov Institute", Gatchina 188300, Russia

<sup>9</sup>St. Petersburg Electrotechnical University "LETI", Prof. Popov Str. 5, St. Petersburg, 197376, Russia

<sup>10</sup>Joint Quantum Institute, National Institute of Standards and Technology and the University of Maryland, Gaithersburg, Maryland 20742, USA

<sup>11</sup>School of Physics, University of New South Wales, Sydney, New South Wales 2052, Australia

<sup>12</sup>Erlangen Centre for Astroparticle Physics (ECAP), Erwin-Rommel-Straße 1, 91058 Erlangen, Germany

<sup>13</sup>Lawrence Livermore National Laboratory, 7000 East Avenue, Livermore, CA 94550, USA

<sup>14</sup>Ulsan National Institute of Science and Technology, 50 UNIST-gil, Ulsan, South Korea

<sup>15</sup>Physikalisch-Technische Bundesanstalt, Bundesallee 100, 38116 Braunschweig, Germany

<sup>16</sup>Braunschweig University of Technology, Universitätsplatz 2, 38106 Braunschweig, Germany

<sup>17</sup>Peter the Great St.Petersburg Polytechnic University, 195251 St. Petersburg, Russia

<sup>18</sup>Institut für Optik und Quantenelektronik, Friedrich-Schiller-Universität Jena, Max-Wien-Platz 1, 07743 Jena, Germany

<sup>19</sup>Helmholtz-Institut Jena, Fröbelstieg 3, 07743 Jena, Germany

<sup>20</sup>GSI Helmholtzzentrum für Schwerionenforschung, Planckstraße 1, 64291 Darmstadt, Germany

(Dated: December 21, 2024)

We measured the  $L$ -shell soft X-ray fluorescence of Fe XVII ions in an electron beam ion trap following resonant photo-excitation using synchrotron radiation provided by the P04 beamline at PETRA III. Special attention is paid to two  $2p - 3d$  transitions, the 3C and 3D lines that are essential plasma diagnostics tools for astrophysics. Their resulting oscillator-strength ratio,  $f(3C)/f(3D) = 3.09(8)(6)$ , is three times more accurate than previous results. The present ratio clearly departs by approximately 5-sigmas from the newest *ab initio* calculations but confirms previous laboratory measurements and astrophysical observations. A ten thousand-fold reduction in excitation-photon intensity and ten times higher spectral resolution allow us to exclude current explanations, reinstating a forty-year-old atomic-physics puzzle.

Space X-ray observatories, such as *Chandra* and *XMM-Newton*, resolve  $L$ -shell transitions of iron dominating the spectra of many hot astrophysical objects [1–4]. Some of the brightest lines arise from Fe XVII (Ne-like iron) around 15 Å: the resonance line 3C ( $[(2p^5)_{1/2} 3d_{3/2}]_{J=1} \rightarrow [2p^6]_{J=0}$ ) and the intercombination line 3D ( $[(2p^5)_{3/2} 3d_{5/2}]_{J=1} \rightarrow [2p^6]_{J=0}$ ). They are crucial for plasma diagnostics of electron temperatures, elemental abundances, ionization conditions, velocity turbulences, and opacities [5–14]. However, for the past four decades, their observed intensity ratios persistently disagree with advanced plasma models, diminishing the utility of high-resolution X-ray observations. Several laboratory experiments using electron beam ion trap (EBIT) and tokamak devices scrutinizing plausible astrophysical and plasma physics explanations as well as the underlying atomic theory [15–22] have shown clear departures from predictions but confirmed astrophysical observations [18, 19, 23]. This

has fueled a long-lasting controversy on the cause being a lack of understanding of astrophysical plasmas, or inaccurate atomic data.

A direct probe of these lines using an EBIT at the Linac Coherent Light Source (LCLS) X-ray free-electron laser (XFEL) found again their oscillator-strength ratio  $f(3C)/f(3D)$  to be lower than predicted, but close to astrophysical observations [24]. Difficulties with the calculations of oscillator strengths in many-electron systems [23–30] were highlighted. Due to the high peak brilliance of the LCLS XFEL, non-linear excitation dynamics [31, 32] or non-equilibrium time evolution [33] might have affected that experiment. An effect of resonance-induced population transfer between Fe XVI and Fe XVII ions was also postulated [34] since the Fe XVI line C ( $[(2p^5)_{1/2} (3s3d)_{5/2}]_{J=3/2} \rightarrow [2p^6 3s]_{J=1/2}$ ) appeared blended with the Fe XVII line 3D. A recent semi-empirical calculation [35] reproduces the LCLS results [24] by fine-tuning

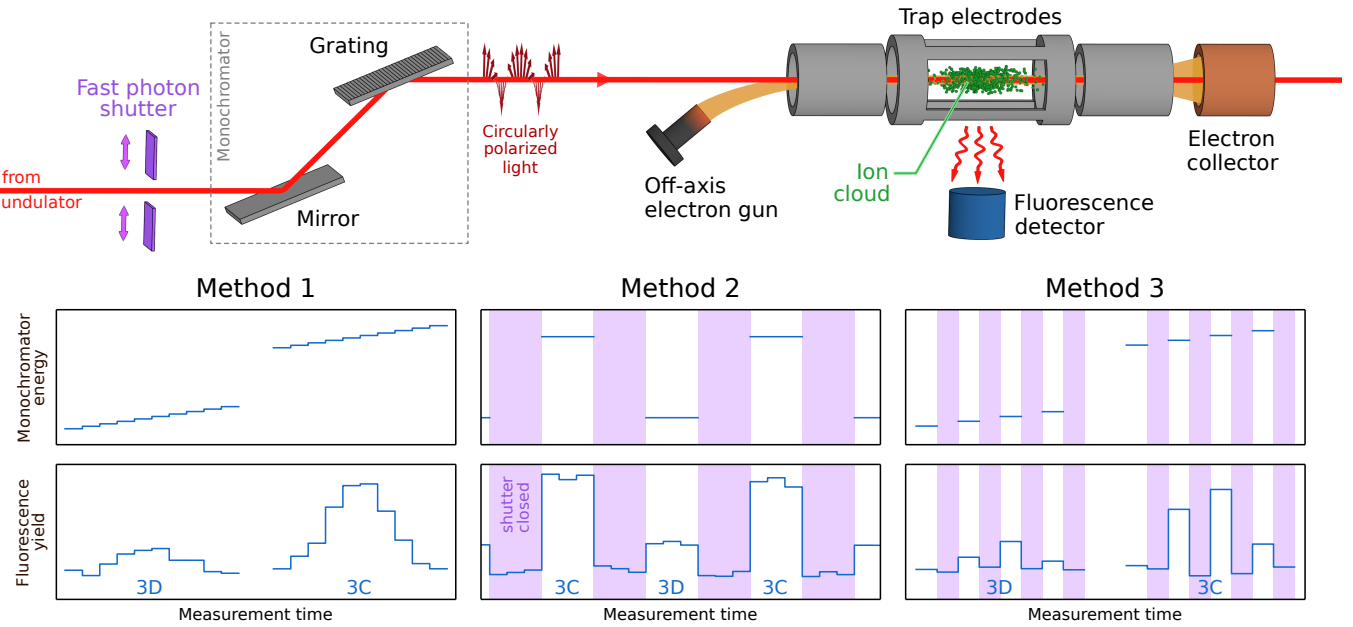


FIG. 1. Upper panel: Experimental setup. An electron beam (orange) aimed at the trap center produces Fe XVII ions, which are then resonantly excited by a monochromatic photon beam (red). Subsequent X-ray fluorescence is registered by a silicon drift detector. Lower panel: Histograms of the fluorescence signal yield versus incident photon energies for three different measurement methods. (1) Lines were scanned across the corresponding energies without using a photon shutter. (2) and (3) the fluorescence was measured at (2) line centroids and (3) over a one-FWHM broad range. In (2) and (3), electron-beam induced background was subtracted by closing a beamline photon shutter cyclically between photon-energy steps (purple areas).

relativistic couplings and orbital relaxation effects, but its validity has been disproved [36].

In this Letter, we report on new measurements of resonantly excited Fe XVI and Fe XVII with a synchrotron source with ten-fold improved spectral resolution and 10,000 lower peak photon flux than in [24], suppressing non-linear dynamical effects [31, 33] and undesired ion population transfers [34]. We also carry out improved large-scale calculations using multi-reference multiconfigurations Dirac-Hartree-Fock (MR-MCDHF) [37, 38] and configuration-interaction (CI) [39, 40] approaches, both showing a 5-sigma departure from our experimental results.

We used the compact PolarX-EBIT [41], in which a monoenergetic electron beam emitted by an off-axis cathode (see Fig. 1) is compressed by a magnetic field. In the trap center it intersects a beam of iron-pentacarbonyl molecules, dissociating them, and producing highly charged Fe ions by collisions. These ions stay radially confined by the negative space charge of the  $\sim 2$  mA, 1610 eV ( $\approx 3$  times the Fe XVI ionization potential) electron beam, and axially by potentials applied to surrounding electrodes. Monochromatic, circularly polarized photons from the P04 beamline [42] at the PETRA III synchrotron photon source enter through the electron gun, irradiate the trapped ions, and exit through the collector aperture. They can resonantly excite X-ray transitions on top of the strong electron-induced background due to ionization, recombination, and excitation processes. A silicon drift detector (SDD) registers these emissions side-on.

By scanning the P04 monochromator between 810 and 830 eV, we excite the Fe XVII lines 3C and 3D, as well as the Fe XVI lines B ( $[(2p^5)_{1/2}(3s3d)_{3/2}]_{J=1/2} \rightarrow [2p^63s]_{J=1/2}$ ) and C. They are also non-resonantly excited by electron-impact excitation as the electron beam energy is well above threshold [20, 22]. This leads to a constant X-ray background at the same energies as the photoexcited transitions. In our earlier work [24], we registered fluorescence in time coincidence with the sub-picosecond long LCLS pulses of  $\approx 10^{11}$  photons each at 120 Hz, rejecting this background. At P04, in contrast, 50-ps-long bunches of only  $\approx 10^3$  photons with a 60-MHz repetition rate could not be resolved in time by the detector from the continuous background, yielding a signal-to-background ratio of only  $\sim 5\%$ . To subtract the background we used a shutter to cyclically turn on and off the P04 photon beam, which reached with a (50  $\mu$ m) slit width a spectral resolution of  $E/\Delta E \approx 10000$ , ten-to-fifteen times higher than that of *Chandra* and *XMM-Newton* grating spectrometers [43, 44], and ten times better than in our previous LCLS experiment [24]. It separates 3C and 3D with meV accuracy to  $\Delta E_{3C-3D} = 13.398(1)$  eV, and resolves for the first time the Fe XVII 3D line from the Fe XVI C one, at  $\Delta E_{3D-C} = 154.3(1.3)$  meV. Therefore, the 3C/3D intensity ratio could be obtained without having to infer the (in [24] still unresolved) contribution of Fe XVI line C from the intensity of the well-resolved Fe XVI line A. This largely reduces systematic uncertainties and excludes resonance-induced population transfer [34], a recently found mechanism that may have af-

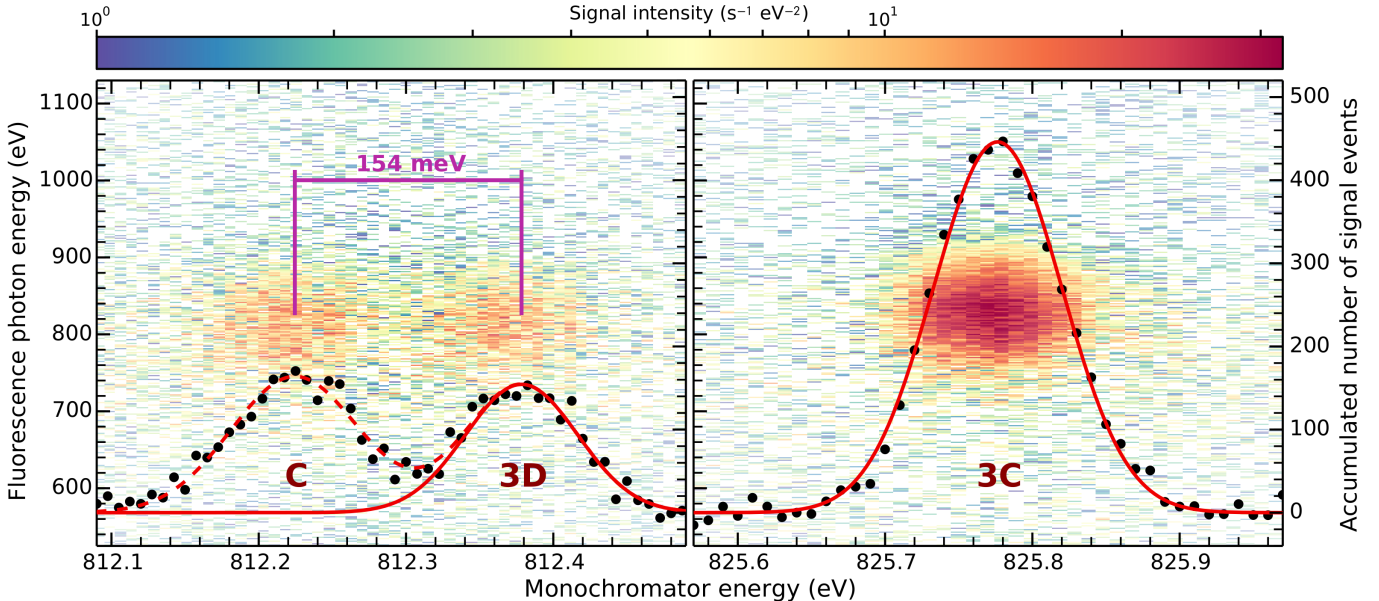


FIG. 2. Fluorescence photon yield and energy vs. excitation-photon energy for the Fe XVI C, Fe XVII 3C, and 3D transitions recorded by a silicon-drift detector. Black dots: Total fluorescence within a 50-eV region of interest. Red solid lines: Fits to 3C and 3D. Red dashed line: Fit to C.

fected the LCLS result [24].

We systematically measured the 3C/3D oscillator-strength ratio by three different techniques, shown in Fig. 1. In *method 1* we did not use the photon shutter, but repeatedly scanned the lines C and 3D (812.0 to 812.5 eV), as well as 3C (825.5 to 826.0 eV), in both cases using scans of 100 steps with 20-s exposure each, see Fig. 2. The fluorescence signal over a 50-eV wide photon-energy region of interest (ROI) including 3C, 3D, and C was recorded versus the incident photon energy. By fitting Gaussians, we obtain line positions, widths, and yields, and modeled the electron-impact background as a smooth linear function [22]. The ratio of 3C and 3D areas is then proportional to the oscillator-strength ratio [32]. However, the low signal-to-background ratio and long measurement times can change the background, and cause systematic uncertainties. In *method 2*, we fixed the monochromator energy to the respective centroids of C, 3D, and 3C found with *method 1*, and cyclically opened and closed the shutter for equal periods of 20 s to determine the background. The background-corrected fluorescence yields at the line peaks were multiplied with the respective linewidths from *method 1*, to obtain the 3C/3D ratio. Still, slow monochromator shifts from the selected positions could affect the results. In a variation of this approach, in *method 3*, we scanned about the full-width-at-half-maximum (FWHM) of C, 3D, and 3C in 33 steps with on-off exposures of 20 s. This approach reduces the effect of possible monochromator shifts. After background subtraction, we fit Gaussians to the lines of interest fixing their widths to values from *method 1*.

All three methods share systematic uncertainties caused by energy-dependent filter transmission and detector efficiency ( $\sim 1\%$ ) and by the incident photon beam flux varia-

tion ( $\sim 2\%$ ). Additionally, for *method 1*, we estimate systematic uncertainties from background ( $\sim 1.2\%$ ) and ROI selection ( $\sim 2.7\%$ ). In *method 2*, possible monochromator shifts from (set) line centroids and widths taken from *method 1* cause a systematic uncertainty of  $\sim 3.5\%$ . Analogously, for *method 3* we estimate a  $\sim 3\%$  uncertainty due to the use of linewidth constraints from *method 1*. The weighted average of all three methods is  $f(3C)/f(3D) = 3.09(8)_{\text{sys}}(6)_{\text{stat}}$ , see Fig. 3. The 3C/3D oscillator-strength ratios from each method and their systematic uncertainties appear in the Supplementary Material. Note that the circular polarization of the photon beam does not affect these results, since 3C and 3D (both  $\Delta J = 1$ ) share the same angular emission characteristics [22, 24, 55, 56].

Calculations using a density-matrix approach pointed to a possible non-linear response of the excited populations in [24] causing a reduction of the observed oscillator-strength ratio [31, 32]. In the present work, the peak photon flux is more than four orders of magnitude lower than in [24], completely suppressing those effects [31–33], which require intensities greater than  $\approx 10^{11} \text{ W cm}^{-2}$ . While the statistical nature of the self-amplified spontaneous emission process at LCLS could conceivably have caused non-linearities in [24], its conclusions are now substantiated with reduced uncertainty. Given the closely-related solar opacity crisis [12, 14], basically pointing to too low oscillator strengths in the used Rosseland mean opacities, the present results call for efforts in further developing the theory of many-electrons systems. The present disagreement with our accurately measured one-hole excitations in a filled *L*-shell is a hint of persistent problems in the usual approximations.

Here we carried out relativistic calculations using a very-

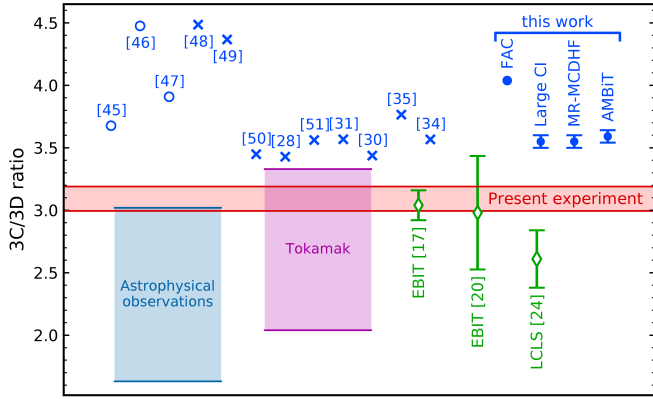


FIG. 3. Present experimental 3C/3D ratios compared with previous predictions and experiments. Red band: Combined results of three different methods. Blue circles: Values from databases [45–47]. Blue crosses: Predictions [28, 30, 31, 34, 35, 48–51]. Blue solid circles: Present FAC [52], large-scale CI [39], MR-MCDHF [37, 38], and AMBiT [40] calculations. Light blue band: range of ratios observed in the Sun [53, 54], Capella [3, 4], and NGC4636 [7]. Purple band: Tokamak results spread [19]. Open green diamonds: previous EBIT results [17, 20, 24]. Note that the ratio from Ref.[20] can be renormalized, bringing its uncertainty closer to that of Ref. [17].

large-scale configuration interaction (CI) method, correlating all ten electrons, including Breit and quantum electrodynamical (QED) [57] corrections. We implemented a message passing interface (MPI) version of the CI code from [39] to increase the number of configurations to over 230,000, saturating the computation in all possible numerical parameters. Basis sets of increasing size are used to check for convergence, with all orbitals up to  $12sp17dfg$  included in the largest version (the contributions of  $n > 12$   $sp$  orbitals are negligible). We start with all possible single and double excitations from the  $2s^22p^6$ ,  $2s^22p^53p$  even and  $2s^22p^53s$ ,  $2s^22p^53d$ ,  $2s2p^63p$ ,  $2s^22p^54d$ ,  $2s^22p^55d$  odd configurations, correlating 8 electrons. We separately calculate triple excitations and fully correlate the  $1s^2$  shell. We also included dominant quadruple excitations and found them negligible. The line strengths  $S$  and 3C/3D oscillator-strength ratio after several computation stages are summarised in the Supplementary Material, which illustrate the small effect of all corrections. Theoretical uncertainties are estimated based on the variance of results from the smallest to largest runs, size of the various effects, and small variances in the basis set construction. We verified that the energies of all 18 states considered, counted from the ground state, agree with the NIST database well within the estimated experimental uncertainty of 0.05%. The theoretical 3C-3D energy difference of 13.44 eV is in agreement with the experiment to 0.3%. For the natural linewidths, we further evaluated the effect of all other 9 allowed transitions from the 3C and 3D level to the  $2p^53p$  levels, yielding a negligible total of  $1.5 \times 10^{10} s^{-1}$  [0.07%] for the 3C and  $1.4 \times 10^{10} s^{-1}$  [0.2%] for the 3D levels.

We also carried out entirely independent large-scale cal-

culations using the MR-MCDHF approach [38]. First, the  $2s^22p^53s$ ,  $2s^22p^53d$  and  $2s^12p^63p$   $J = 1$  levels were used as reference states to generate the list of configuration state functions with single and double exchanges from all occupied orbitals up to  $12spdfghi$ . Virtual orbitals were added in a layer-by-layer manner. Subsequently, the role of triple excitations was studied by the CI method. In a second step, the multireference list was extended to include all  $J = 1$  odd parity states, generated from the Ne-like ground state by single and double electron exchanges. Monitoring the convergence of the results for the addition of layers of virtual orbits, we arrive at an oscillator-strength ratio of 3.55(5), and to a 3C-3D energy splitting of 13.44(5) eV.

Another full-scale CI calculation was carried out in the particle-hole formalism using AMBiT [40], which agrees with the other CI results. Full details of all calculations can be found in the Supplementary Material.

We emphasize that there are no other known quantum mechanical effects or numerical uncertainties to consider within the CI and MCDHF approaches. With modern computational facilities and MPI codes, we have shown that all other contributions are negligible at the level of the quoted theoretical uncertainties. The significant improvements in experimental and theoretical precision reported here have only further deepened this long-standing problem.

Our present work on possibly the most intensively studied many-electron ion in experiment and theory finally demonstrates the convergence of the atomic calculations on all possible parameters, removing incomplete inclusion of the correlation effects as a potential explanation of this puzzle. Shortcomings of low-precision atomic theory for  $L$ -shell ions had persistently been suggested based on the analysis of high-resolution *Chandra* and *XMM-Newton* data [13, 18, 19, 23, 58]. Similar inconsistencies were recently found in the high-resolution  $K$ -shell X-ray spectra of the Perseus cluster recorded with the *Hitomi* microcalorimeter [59, 60]. Moreover, the newest systematic opacity measurements also highlight serious inconsistencies in the opacity models [12, 14] used to describe the interior of the Sun and stars. The actual accuracy and reliability of the opacity and turbulence velocity diagnostics are therefore still questionable, and with it, the modeling of hot astrophysical plasmas. The upcoming X-ray observatory missions *XRISM* [61] and *Athena* [62] will require improved and quantitatively validated modeling tools to harvest the best possible scientific data. For this, benchmarking atomic theories with laboratory measurements is vital. As for the long-standing Fe XVII oscillator-strength problem, our results may be used to semi-empirically correct spectral models for the interpretation of astrophysical observations.

## ACKNOWLEDGEMENTS

Financial support was provided by the Max-Planck-Gesellschaft (MPG) and Bundesministerium für Bildung und Forschung (BMBF) through project 05K13SJ2. Work by C.

Shah was supported by the Deutsche Forschungsgemeinschaft (DFG) Project No. 266229290 and by an appointment to the NASA Postdoctoral Program at the NASA Goddard Space Flight Center, administered by Universities Space Research Association under contract with NASA. Work by LLNL was performed under the auspices of the U.S. Department of Energy under contract No. DE-AC52-07NA27344. M.A.L. acknowledges support from NASA's Astrophysics Program. The work of M.G.K. and S.G.P. was supported by the Russian Science Foundation under Grant No. 19-12-00157. The theoretical research was supported in part through the use of Information Technologies resources at the University of Delaware, specifically the high-performance Caviness computing cluster. Work by UNIST was supported by the National Research Foundation of Korea (No. NRF-2016R1A5A1013277). J.C.B. acknowledges support from the Alexander von Humboldt Foundation.

S.K. and C.S. contributed equally to this work.

---

\* [steffen.kuehn@mpi-hd.mpg.de](mailto:steffen.kuehn@mpi-hd.mpg.de)  
 † [chintan@mpi-hd.mpg.de](mailto:chintan@mpi-hd.mpg.de); [chintan.d.shah@nasa.gov](mailto:chintan.d.shah@nasa.gov)

[1] F. B. S. Paerels and S. M. Kahn, *Annu. Rev. Astron. Astrophys.* **41**, 291 (2003).

[2] C. R. Canizares, D. P. Huenemoerder, D. S. Davis, D. Dewey, K. A. Flanagan, J. Houck, T. H. Markert, H. L. Marshall, M. L. Schattenburg, N. S. Schulz, *et al.*, *Astrophys. J. Lett.* **539**, L41 (2000).

[3] E. Behar, J. Cottam, and S. M. Kahn, *Astrophys. J.* **548**, 966 (2001).

[4] R. Mewe, A. J. J. Raassen, J. J. Drake, J. S. Kaastra, R. L. J. van der Meer, and D. Porquet, *Astron. Astrophys.* **368**, 888 (2001).

[5] J. H. Parkinson, *Astron. Astrophys.* **24**, 215 (1973).

[6] R. Doron and E. Behar, *Astrophys. J.* **574**, 518 (2002).

[7] H. Xu, S. M. Kahn, J. R. Peterson, E. Behar, F. B. S. Paerels, R. F. Mushotzky, J. G. Jernigan, A. C. Brinkman, and K. Makishima, *Astrophys. J.* **579**, 600 (2002).

[8] N. S. Brickhouse and J. Schmelz, *Astrophys. J. Lett.* **636**, L53 (2005).

[9] J. S. Sanders and A. C. Fabian, *Mon. Notices Royal Astron. Soc.* **412**, L35 (2011).

[10] T. Kallman, A. E. Daniel, H. Marshall, C. Canizares, A. Longinotti, M. Nowak, and N. Schulz, *Astrophys. J.* **780**, 121 (2014).

[11] J. de Plaa, I. Zhuravleva, N. Werner, J. S. Kaastra, E. Churazov, R. K. Smith, A. J. J. Raassen, and Y. G. Grange, *Astron. Astrophys.* **539** (2012).

[12] J. E. Bailey, T. Nagayama, G. P. Loisel, G. A. Rochau, C. Blanckard, J. Colgan, P. Cosse, G. Faussurier, C. Fontes, F. Gilleron, *et al.*, *Nature* **517**, 56 (2015).

[13] P. Beiersdorfer, N. Hell, and J. Lepson, *Astrophys. J.* **864**, 24 (2018).

[14] T. Nagayama, J. E. Bailey, G. P. Loisel, G. S. Dunham, G. A. Rochau, C. Blanckard, J. Colgan, P. Cossé, G. Faussurier, C. J. Fontes, *et al.*, *Phys. Rev. Lett.* **122**, 235001 (2019).

[15] G. V. Brown, P. Beiersdorfer, D. A. Liedahl, K. Widmann, and S. M. Kahn, *Astrophys. J.* **502**, 1015 (1998).

[16] P. Beiersdorfer, S. von Goeler, M. Bitter, and D. B. Thorn, *Phys. Rev. A* **64**, 032705 (2001).

[17] G. V. Brown, P. Beiersdorfer, H. Chen, M. H. Chen, and K. J. Reed, *Astrophys. J. Lett.* **557**, L75 (2001).

[18] P. Beiersdorfer, E. Behar, K. Boyce, G. Brown, H. Chen, K. Gendreau, M.-F. Gu, J. Gygax, S. Kahn, R. Kelley, *et al.*, *Astrophys. J. Lett.* **576**, L169 (2002).

[19] P. Beiersdorfer, M. Bitter, S. Von Goeler, and K. Hill, *Astrophys. J.* **610**, 616 (2004).

[20] G. V. Brown, P. Beiersdorfer, H. Chen, J. H. Scofield, K. R. Boyce, R. L. Kelley, C. A. Kilbourne, F. S. Porter, M. F. Gu, S. M. Kahn, and A. E. Szymkowiak, *Phys. Rev. Lett.* **96**, 253201 (2006).

[21] G. V. Brown and P. Beiersdorfer, *Phys. Rev. Lett.* **108**, 139302 (2012).

[22] C. Shah, J. R. C. López-Urrutia, M. F. Gu, T. Pfeifer, J. Marques, F. Grilo, J. P. Santos, and P. Amaro, *Astrophys. J.* **881**, 100 (2019).

[23] M. F. Gu, *arXiv e-prints*, arXiv:0905.0519 (2009), arXiv:0905.0519 [astro-ph.SR].

[24] S. Bernitt, G. V. Brown, J. K. Rudolph, R. Steinbrugge, A. Graf, M. Leutenegger, S. W. Epp, S. Eberle, K. Kubicek, V. Mackel, *et al.*, *Nature* **492**, 225 (2012).

[25] U. I. Safronova, C. Namba, I. Murakami, W. R. Johnson, and M. S. Safronova, *Phys. Rev. A* **64**, 012507 (2001).

[26] G. X. Chen and A. K. Pradhan, *Phys. Rev. Lett.* **89**, 013202 (2002).

[27] S. D. Loch, M. S. Pindzola, C. P. Ballance, and D. C. Griffin, *J. Phys. B: At., Mol. Opt. Phys.* **39**, 85 (2006).

[28] G.-X. Chen, *Phys. Rev. A* **76**, 062708 (2007).

[29] G. Chen, *Phys. Rev. A* **84**, 012705 (2011).

[30] J. A. Santana, J. K. Lepson, E. Träbert, and P. Beiersdorfer, *Phys. Rev. A* **91**, 012502 (2015).

[31] N. S. Oreshkina, S. M. Cavaletto, C. H. Keitel, and Z. Harman, *Phys. Rev. Lett.* **113**, 143001 (2014).

[32] N. S. Oreshkina, S. M. Cavaletto, C. H. Keitel, and Z. Harman, *J. Phys. B: At., Mol. Opt. Phys.* **49**, 094003 (2016).

[33] S. D. Loch, C. P. Ballance, Y. Li, M. Fogle, and C. J. Fontes, *Astrophys. J. Lett.* **801**, L13 (2015).

[34] C. Wu and X. Gao, *Sci. Rep.* **9**, 7463 (2019).

[35] C. Mendoza and M. A. Bautista, *Phys. Rev. Lett.* **118**, 163002 (2017).

[36] K. Wang, P. Jönsson, J. Ekman, T. Brage, C. Y. Chen, C. F. Fischer, G. Gaigalas, and M. Godefroid, *Phys. Rev. Lett.* **119**, 189301 (2017).

[37] Z. Harman, I. I. Tupitsyn, A. N. Artemyev, U. D. Jentschura, C. H. Keitel, J. R. Crespo López-Urrutia, A. J. González Martínez, H. Tawara, and J. Ullrich, *Phys. Rev. A* **73**, 052711 (2006).

[38] C. F. Fischer, G. Gaigalas, P. J. Ånsson, and J. BieroÅ, *Comput. Phys. Commun.* **237**, 184 (2019).

[39] M. Kozlov, S. Porsey, M. Safronova, and I. Tupitsyn, *Comput. Phys. Commun.* **195**, 199 (2015).

[40] E. V. Kahl and J. C. Berengut, *Comput. Phys. Commun.* **238**, 232 (2019).

[41] P. Micke, S. Kühn, L. Buchauer, J. R. Harries, T. M. Bücking, K. Blaum, A. Cieluch, A. Egl, D. Hollain, S. Kraemer, *et al.*, *Rev. Sci. Instrum.* **89**, 063109 (2018).

[42] J. Viefhaus, F. Scholz, S. Deinert, L. Glaser, M. Ilchen, J. Seltmann, P. Walter, and F. Siewert, *Nucl. Instrum. Methods Phys. Res., Sect. A* **710**, 151 (2013).

[43] J. Den Herder, A. Brinkman, S. Kahn, G. Branduardi-Raymont, K. Thomsen, H. Aarts, M. Audard, J. Bixler, A. den Boggende, J. Cottam, *et al.*, *Astron. Astrophys.* **365**, L7 (2001).

[44] C. R. Canizares, J. E. Davis, D. Dewey, K. A. Flanagan, E. B. Galton, D. P. Huenemoerder, K. Ishibashi, T. H. Markert, H. L. Marshall, M. McGuirk, *et al.*, *Publ. Astron. Soc. Pac* **117**, 1144 (2005).

[45] A. Kramida, Yu. Ralchenko, J. Reader, and and NIST ASD Team, NIST Atomic Spectra Database (ver. 5.6.1), [Online]. Available: <https://physics.nist.gov/asd> [2019, September 6]. National Institute of Standards and Technology, Gaithersburg, MD. (2018).

[46] J. S. Kaastra, R. Mewe, and H. Nieuwenhuijzen, in *11th Colloq. on UV and X-ray Spectroscopy of Astrophysical and Laboratory Plasmas*, edited by K. Yamashita and T. Watanabe (Tokyo: Universal Academy Press, 1996) pp. 411–414.

[47] A. R. Foster, L. Ji, R. K. Smith, and N. S. Brickhouse, *Astrophys. J.* **756**, 128 (2012).

[48] A. Bhatia and G. Doschek, *At. Data Nucl. Data Tables* **52**, 1 (1992).

[49] G.-X. Chen, A. K. Pradhan, and W. Eissner, *J. Phys. B: At., Mol. Opt. Phys.* **36**, 453 (2003).

[50] C. Dong, L. Xie, S. Fritzsche, and T. Kato, *Nucl. Instrum. Methods Phys. Res., Sect. B* **205**, 87 (2003), 11th International Conference on the Physics of Highly Charged Ions.

[51] P. Jönsson, P. Bengtsson, J. Ekman, S. Gustafsson, L. Karlsson, G. Gaigalas, C. F. Fischer, D. Kato, I. Murakami, H. Sakaue, *et al.*, *At. Data Nucl. Data Tables* **100**, 1 (2014).

[52] M. F. Gu, *Can. J. Phys.* **86**, 675 (2008).

[53] R. Blake, T. Chubb, H. Friedman, and A. Unzicker, *Astrophys. J.* **142**, 1 (1965).

[54] D. L. McKenzie, P. B. Landecker, R. M. Broussard, H. R. Rugge, R. M. Young, U. Feldman, and G. A. Doschek, *Astrophys. J.* **241**, 409 (1980).

[55] V. V. Balashov, A. N. Grum-Grzhimailo, and N. M. Kabachnik, *Polarization and Correlation Phenomena in Atomic Collision* (Kluwer Academic/ Plenum publishers, 2000).

[56] C. Shah, H. Jörg, S. Bernitt, S. Dobrodey, R. Steinbrügge, C. Beilmann, P. Amaro, Z. Hu, S. Weber, S. Fritzsche, *et al.*, *Phys. Rev. A* **92**, 042702 (2015).

[57] I. I. Tupitsyn, M. G. Kozlov, M. S. Safronova, V. M. Shabaev, and V. A. Dzuba, *Phys. Rev. Lett.* **117**, 253001 (2016).

[58] H. Netzer, *Astrophys. J.* **604**, 551 (2004).

[59] Hitomi Collaboration *et al.*, *Nature* **535**, 117 (2016).

[60] Hitomi Collaboration *et al.*, *Publ. Astron. Soc. Jpn.* **70**, 12 (2018).

[61] M. Tashiro, H. Maejima, K. Toda, R. Kelley, L. Reichenthal, J. Lobell, R. Petre, M. Guainazzi, E. Costantini, M. Edison, *et al.*, *Proc. SPIE* **10699**, 1069922 (2018).

[62] D. Barret, T. L. Trong, J.-W. Den Herder, L. Piro, X. Barcons, J. Huovelin, R. Kelley, J. M. Mas-Hesse, K. Mitsuda, S. Paltani, *et al.*, in *Space Telescopes and Instrumentation 2016: Ultraviolet to Gamma Ray*, Vol. 9905 (International Society for Optics and Photonics, 2016) p. 99052F.

# High-resolution Photo-excitation Measurements Exacerbate the Long-standing Fe XVII-Emission Problem: Supplementary Material

## I. EXPERIMENT AND DATA ANALYSIS

TABLE I. Comparison between experimental values and theoretical predictions of the 3C/3D oscillator strength ratio and relative line energy positions achieved within this work.

	Experiment	CI	MCDHF	AMBiT
3C/3D oscillator strength ratio	3.09(8) <sub>sys</sub> (6) <sub>stat</sub>	3.55(5)	3.55(5)	3.59(5)
Energy 3C (eV)		825.67	825.88(5)	825.923
Energy 3D (eV)		812.22	812.44(5)	812.397
ΔEnergy 3C-3D (eV)	13.398(1)	13.44(5)	13.44(5)	13.526
ΔEnergy 3D-C (eV)	0.1543(13)			
Natural linewidth 3C (meV)		14.74(3)	14.75(3)	14.90
Natural linewidth 3D (meV)		4.02(5)	4.01(6)	4.04

### A. Individual methods data and their uncertainties

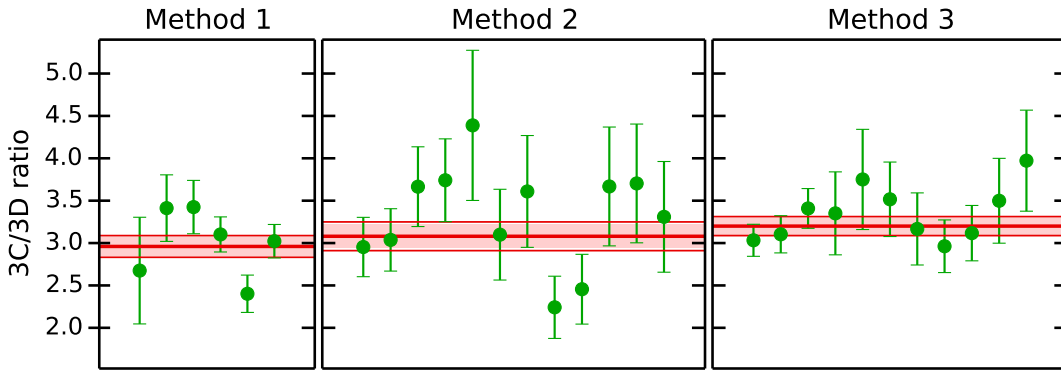


FIG. 1. Experimental 3C/3D ratio for the three different methods. The individual measurements are shown as solid green circles. The weighted mean experimental values and associated  $1-\sigma$  statistical and systematic uncertainties are indicated as red band.

TABLE II. 3C/3D oscillator strength ratios obtained from three different measurement methods and their statistical and systematic uncertainties.

3C/3D oscillator strength ratio	Method 1	Method 2	Method 3
Uncertainty Budget			
Statistical	0.106	0.140	0.095
Systematics due to:			
(1) ROI width selection on 2D histogram (Fig. 2 of the main paper)	0.030		
(2) ROI centroid selection on 2D histogram	0.044		
(3) Filter transmission and efficiency of the detector	0.030	0.031	0.032
(4) Time-dependent background variation due to the electron-impact excitation	0.036		
(5) Monochromator shifts in the (set) energy position	0.092		
(6) Linewidth constraints in Gaussian fits			0.048
Total systematic uncertainty	0.071	0.097	0.058
Total (statistical + systematic) uncertainties	0.127	0.170	0.111
Common systematics for all three methods:			
Flux variation of the incident photon beam at P04/PETRA III			0.0618
<b>Final 3C/3D oscillator strength ratio</b>	<b><math>3.09 \pm 0.08_{\text{stat.}} \pm 0.06_{\text{sys.}}</math></b>		

### B. Resolving Fe XVII 3D and Fe XVII C lines

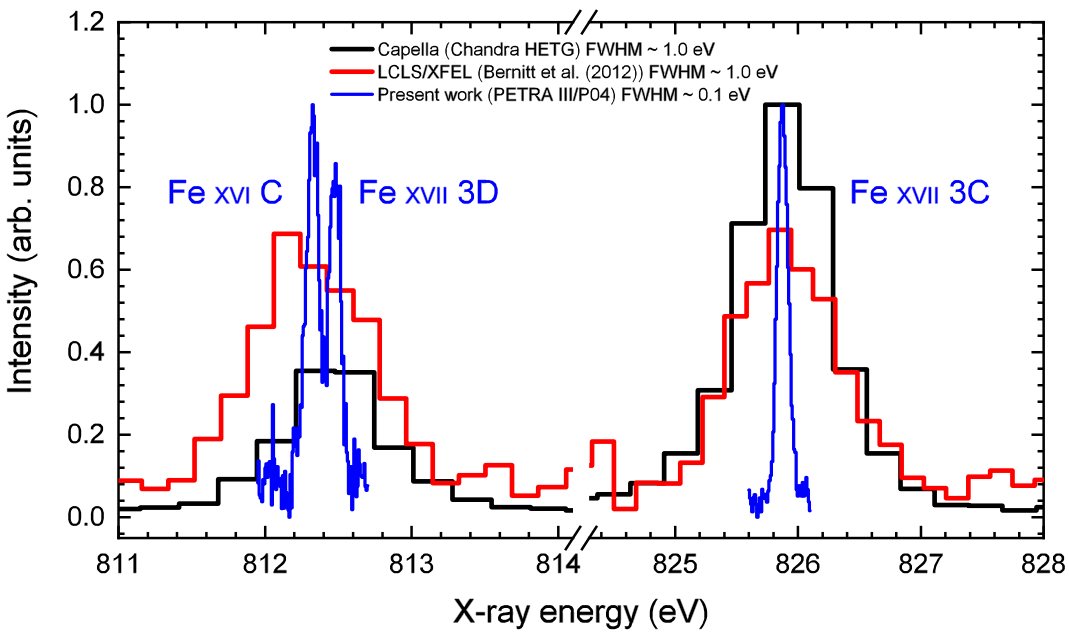


FIG. 2. Spectral resolution comparison between the present work at PETRA III/P04, our previous work at LCLS/XFEL [1], and the high resolution *Chandra* High Energy Transmission Grating (HETG) [2] spectrum of Capella [ObsId: 1103]. In this work, for the first time, we have resolved previously-blended Fe XVI C from Fe XVII 3D line, which are 154.3(1.3) meV apart from each other. This enables us to obtain the line intensity ratio of Fe XVII 3C and 3D without having to subtract the contribution of the Fe XVI C line, in contrast to all other previous works. Moreover, this has largely reduced the systematic uncertainties and eliminated the need for taking resonance-induced population transfer [3] into account, which may have affected the accuracy of our LCLS work [1].

## II. CALCULATIONS OF 3C AND 3D OSCILLATOR STRENGTHS

### A. Very large-scale CI calculations

We start from the solution of the Dirac-Hartree-Fock equations in the central field approximation to construct the one-particle orbitals. The calculations are carried out using a configuration interaction (CI) method, correlating all 10 electrons. The Breit interaction is included in all calculations. The QED effects are included following Ref. [4]. The basis sets of increasing sizes are used to check for convergence of the values. The basis set is designated by the highest principal quantum number for each partial wave included. For example, [5spd $f$ 6g] means that all orbitals up to  $n = 5$  are included for the  $spd$  $f$  partial waves and  $n = 5, 6$  orbitals are included for the  $g$  partial waves. We find that the inclusion of the  $6, 7h$  orbitals does not modify the results of the calculations and omit higher partial waves. The CI many-electron wave function is obtained as a linear combination of all distinct states of a given angular momentum  $J$  and parity [5]:

$$\Psi_J = \sum_i c_i \Phi_i. \quad (1)$$

The energies and wave functions are determined from the time-independent multiparticle Schrödinger equation  $H\Phi_n = E_n \Phi_n$ .

We start with all possible single and double excitations to any orbital up to 5spd $f$ 6g from the  $2s^22p^6$ ,  $2s^22p^53p$  even and  $2s^22p^53s$ ,  $2s^22p^53d$ ,  $2s2p^63p$ ,  $2s^22p^54d$ ,  $2s^22p^55d$  odd configurations, correlating 8 electrons. We verified that inclusion of the  $2s2p^63s$ ,  $2s^22p^54f$ ,  $2s^22p^55f$  even and  $2s2p^64p$ ,  $2s^22p^54s$ , and  $2s^22p^55s$  odd configurations as basic configurations have negligible effect on either energies of relevant matrix elements.

The only unusually significant change in the ratio, by 0.07, is due to the inclusion of the  $2s^22p^33d^3$  and  $2p^53d^3$  configurations. These are obtained as double excitations from the  $2s^22p^53d$  odd configuration, prompting the inclusion of the  $2s^22p^54d$ ,  $2s^22p^55d$  to the list of the basic configurations.

Contributions to the energies of Fe<sup>16+</sup> calculated with different size basis sets and a number of configurations are listed in Table III. The results are compared with experimental data from the NIST database [6] and from a revised analysis of the experimental data [7]. We use LS coupling and NIST data term designations for comparison purposes, but note that  $jj$  coupling would be more appropriate for this ion. Contributions to the E1 reduced matrix elements  $D(3D) = D(2p^6 1S_0 - 2p^5 3d^3 D_1)$  and

TABLE III. Contributions to the energies of Fe<sup>16+</sup> calculated with increased size basis sets and a number of configurations. The results are compared with experiment. All energies are given in cm<sup>-1</sup> with exception of the last line that shows the difference of the 3C and 3D energies in eV. The basis set is designated by the highest quantum number for each partial wave included. For example, 12spd $f$ g means that all orbitals up to  $n = 12$  are included for  $spd$  $f$  partial waves. Contributions from triple excitations, excitations from the  $1s^2$  shells, and QED contributions are given separately.

Configuration	Expt. [6]	Expt. [7]	[5spd $f$ 6g]	Triples	$1s^2$	$+[12spdfg]$	$+[17dfg]$	QED	Final	Diff. [6]	Diff. [7]	Diff. [7]
$2p^6$ $^1S_0$	0	0	0	0	0	0	0	0	0	0	0	0
$2p^53p$ $^3S_1$	6093450	6093295	6087185	6	254	3876	772	67	6092159	1291	1136	0.02%
$2p^53p$ $^3D_2$	6121690	6121484	6116210	-21	24	2886	701	43	6119842	1848	1642	0.03%
$2p^53p$ $^3D_3$	6134730	6134539	6129041	-23	25	3015	711	94	6132864	1866	1675	0.03%
$2p^53p$ $^1P_1$	6143850	6143639	6138383	-11	41	2825	704	82	6142025	1825	1614	0.03%
$2p^53s$ 2	5849490	5849216	5842248	-10	108	3408	735	787	5847276	2214	1940	0.03%
$2p^53s$ 1	5864770	5864502	5857770	-10	70	3303	708	784	5862626	2144	1876	0.03%
$2p^53s$ 1	5960870	5960742	5953697	-10	74	3364	717	1042	5958883	1987	1859	0.03%
$2p^53d$ $^3P_1$	6471800	6471640	6466575	-11	16	2384	665	87	6469717	2083	1923	0.03%
$2p^53d$ $^3P_2$	6486400	6486183	6481385	-13	16	2250	658	86	6484383	2017	1800	0.03%
$2p^53d$ $^3F_4$	6486830	6486720	6482549	-12	27	1745	622	97	6485028	1802	1692	0.03%
$2p^53d$ $^3F_3$	6493030	6492651	6488573	-14	26	1740	607	84	6491016	2014	1635	0.03%
$2p^53d$ $^1D_2$	6506700	6506537	6502481	-17	21	1696	627	88	6504895	1805	1642	0.03%
$2p^53d$ $^3D_3$	6515350	6515203	6511163	-18	18	1762	604	87	6513617	1733	1586	0.02%
$2p^53d$ $^3D_1$	6552200	6552503	6548550	-16	-3	1747	616	134	6551029	1171	1474	0.02%
$2p^53d$ $^3F_2$	6594360	6594309	6589977	-16	22	1729	629	335	6592676	1684	1633	0.02%
$2p^53d$ $^3D_2$	6600950	6600998	6596316	-17	14	1947	641	334	6599235	1715	1763	0.03%
$2p^53d$ $^1F_3$	6605150	6605185	6600744	-17	19	1803	610	343	6603501	1649	1684	0.03%
$2p^53d$ $^1P_1$	6660000	6660770	6656872	-8	-52	1743	619	288	6659462	538	1308	0.02%
3C-3D	13.3655	13.4234	13.4302	0.0009	-0.0061	-0.0005	0.0004	0.0191	13.4440	-0.0785	-0.0206	0.15%

TABLE IV. Contributions to the  $E1$  reduced matrix elements  $D(3D) = D(2p^6 \ ^1S_0 - 2p^5 3d \ ^3D_1)$  and  $D(3C) = D(2p^6 \ ^1S_0 - 2p^5 3d \ ^1P_1)$  (in a.u.) and the ratio of the respective oscillator strengths  $R$ . See caption of Table III for designations.  $L$  and  $V$  rows compared results obtained in length and velocity gauges for the  $[12spdfg]$  basis. All other results are calculated using the length gauge. Transition rates are listed in the last row in  $s^{-1}$ .

		$D(3C)$	$D(3D)$	Ratio
$[5spdf6g]$		0.33492	0.17842	3.582
$[5spdf6g]$	+Triples	0.33493	0.17841	3.583
	Triples	0.00001	-0.00001	
$[5spdf6g]$	+ $1s^2$	0.33480	0.17849	3.577
	$1s^2$	-0.00012	0.00007	
$[12spdfg]$	$L$	0.33527	0.17884	3.573
	$V$	0.33551	0.17894	3.574
$+[12spdfg]$		0.00036	0.00042	
$+[17dfg]$		-0.00001	0.00001	
QED		-0.00017	0.00030	
Final		0.33498	0.17921	3.552
Recomm.				3.55(5)
Transition rate		$2.238 \times 10^{13}$	$6.098 \times 10^{12}$	

$D(3C) = D(2p^6 \ ^1S_0 - 2p^5 3d \ ^1P_1)$  and the ratio of the respective oscillator strengths

$$R = \left( \frac{D(3C)}{D(3D)} \right)^2 \times \frac{\Delta E(3C)}{\Delta E(3D)}$$

are listed in Table IV. The energy ratio is 1.01655.

We include a very wide range of configurations obtained by triple excitations from the basic configurations as well as excitations from the  $1s^2$  shell and find negligible corrections to both energies and matrix elements as illustrated by Tables III and IV. These contributions are listed as “Triples” and “ $1s^2$ ” in both tables. A significant increase of the basis set from  $[5spdf6g]$  to  $[12spdfg]$  improves the agreement of energies with experiment but gives a very small, -0.009, contribution to the ratio. We find that the weights of the configurations containing  $12fg$  orbitals are several times higher than those containing  $12spd$  orbitals, so we expand the basis to include more  $dfg$  orbitals. We also include  $2s^2 2p^3 nd^3$  and  $2p^5 nd^3$  configurations up to  $n = 14$ . The contributions to the energies of the orbitals with  $n = 13 - 17$  are 3 – 5 times smaller than those with  $n = 6 - 12$ , clearly showing the convergence of the values with the increase of the basis set. The effect on the ratio is negligible. The uncertainty of the NIST database energies,  $3000 \text{ cm}^{-1}$  is larger than our differences with the experiment. The energies from the revised analysis of  $\text{Fe}^{16+}$  spectra [7] are estimated to be accurate to about  $90 \text{ cm}^{-1}$  and the scatter of the differences of different levels with the experiment is reduced. The last line of Table III shows the difference of the  $3C$  and  $3D$  energies in eV, with the final value  $13.44(5)$  eV. We explored several different ways to construct the basis set orbitals. While the final results with an infinitely large basis set and complete configurations set should be identical, the convergence properties of the different basis sets vary, giving about 0.04 difference in the ratio and 0.04 eV in the  $3C - 3D$  energy difference at the  $12spdfg$  level. Therefore, we set an uncertainty of the final value of the ratio to be 0.05. As an independent test of the quality and completeness of the current basis set, we compare the results for  $D(3C)$  and  $D(3D)$  obtained in length and velocity gauges for the  $[12spdfg]$  basis, see rows  $L$  and  $V$  in Table IV. The difference in the results is only 0.001. The final results for the line strengths  $S$  and the  $3C/3D$  oscillator

TABLE V. Contributions to the  $3C$  and  $3D$  line strengths  $S$  and the  $3C/3D$  oscillator strength ratios (energy ratio 1.01655 is used). Energies in eV, transition rates  $A$  in  $s^{-1}$  and natural linewidths  $\Gamma$  in meV are listed in the last three rows of the tables.

	$S(3C)$	$S(3D)$	Ratio
Small basis	0.11217	0.03183	3.582
Medium basis	0.11241	0.03198	3.573
Large basis	0.11240	0.03199	3.572
+ triple excitations	0.11241	0.03198	3.573
+ $1s^2$ shell excitations	0.11233	0.03201	3.567
+QED	0.11221	0.03212	3.552
Final	0.1122(2)	0.0321(4)	3.55(5)
Energies (eV)	825.67	812.22	
$A \text{ (s}^{-1}\text{)}$	$2.238(4) \times 10^{13}$	$6.10(7) \times 10^{12}$	
$\Gamma \text{ (meV)}$	14.74(3)	4.02(5)	

strength ratio after several stages of computations are summarised in Table V, which clearly illustrates a very small effect of all corrections.

This work was supported in part by U.S. NSF Grant No. PHY-1620687 and RFBR grants No. 17-02-00216 and No. 18-03-01220.

### B. Multiconfigurations Dirac-Hartree-Fock calculations

In the multiconfiguration Dirac-Hartree-Fock (MCDHF) method, similarly to the CI approach outlined in the previous section, the many-electron state is given as an expansion in terms of a large set of  $jj$ -coupled configuration state functions [see Eq. (1)]. In contrast to the CI calculations, in the case of MCDHF, the single-electron wave functions (orbitals) are self-consistently optimized. We use the method in one of its most recent implementations, namely, applying the GRASP2018 code package [8]. For the virtual orbitals, the optimization of the orbitals was done in a layer-by-layer approach, i.e. when adding a new layer of orbitals (in our case, orbitals in the same shell) in the configuration expansions, the lower-lying single-electron functions are kept frozen.

In a first set of calculations, we use the  $2s^22p^6$  configuration for the ground state and the  $2s^22p^53s$ ,  $2s^22p^53d$ , and  $2s^12p^63p$   $J = 1$  odd configurations for the excited states to generate the configuration lists. Single and double electron exchanges from

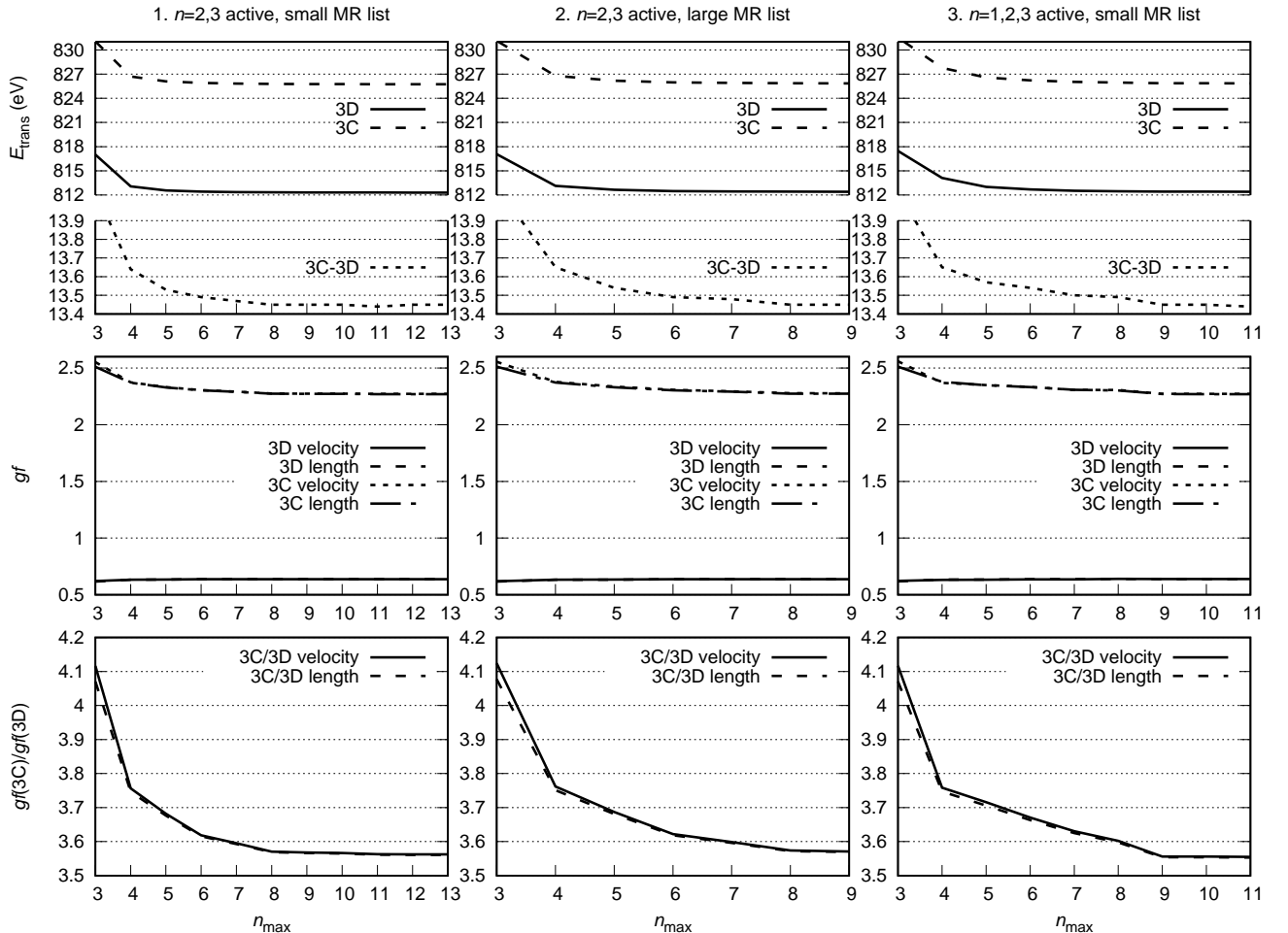


FIG. 3. Convergence of the MCDHF calculations: The X-ray transition energies of the 3C and 3D lines, their difference, the weighted oscillator strengths  $gf$  and their ratio vs. the maximal principal quantum number  $n_{\max}$  used. Oscillator strengths are given both in the relativistic length (Babushkin) and velocity (Coulomb) gauges to numerically control gauge invariance. The different columns display results from different sets of calculations, as described in the text.

the  $n = 2, 3$  spectroscopic (occupied) orbitals were taken into account up to virtual orbitals  $n_{\max}spdfg$ , where the maximal principal quantum number  $n_{\max}$  is varied in the computations to study the convergence of the results. Such an approach is helpful in estimating the final theoretical uncertainty. Test calculations also using virtual orbitals with  $h$  and  $i$  symmetry have shown that these high angular momenta do not play a noticeable role. The ground and excited states were treated separately, i.e. two independently optimized sets of orbitals were used. After these multireference MCDHF calculations, the possible effects of further higher-order electron exchanges were included in a subsequent step, when a CI calculation was performed with the extended configuration lists (triple excitations from the multireference states up to  $n = 4$  orbitals, yielding approx. 800 thousand configurations for  $n_{\max} = 13$ ), employing the radial wave functions obtained from the previous MCDHF calculations. Furthermore, the effects of the frequency-independent Breit relativistic electron interaction operator, the normal and specific mass shift, and approximate radiative corrections are accounted for (see [8] and references therein). The QED effects have been included in the calculation of transition energies (which also enter the oscillator strengths), however, not in the electric dipole matrix elements, as such corrections are anticipated to be on the 1% level and thus can be neglected. The oscillator strengths were evaluated with the biorthogonal basis sets, each optimized separately for the ground- and excited states, to include orbital relaxation effects. The results of these calculations are presented in the first column of Fig. 3. The bottom panel shows that the oscillator strength ratio is converged from  $n_{\max} = 9$  on.

In a subsequent set of calculations, the multireference set describing the ground and excited levels were expanded to include all  $J = 0$  even and  $J = 1$  odd states with 1 or 2 electrons in the M shell. The maximal principal quantum number of the virtual orbitals was set to 9 to limit the computational expense of calculations. Results are shown in the 2nd column of Fig. 3. In a third setting, calculations were performed with the smaller multireference list as described in the previous paragraph, however, with all spectroscopic orbitals (those with  $n = 1, 2, 3$ ) included in the active set of orbitals when generating the configuration list. With the triple electron exchanges also included, this procedure yielded approx. 1.2 million configurations in the description of the excited states. The energies and strengths are shown in the last column of the figure. The converged 3C/3D oscillator strength ratios agree well for all 3 calculations. Comparing the different results, the final value for the ratio is 3.55(5), which agrees well with earlier large-scale MCDHF results [1, 9], and also with the results of the other theoretical methods described in this Supplement. For the difference of the energies of the 3C and 3D lines – which can be more accurately determined in the experiment than the absolute X-ray transition energies – we obtain 13.44(5) eV.

### C. AMBiT: particle-hole CI method calculations

A separate CI calculation of the 3C and 3D lines in  $\text{Fe}^{16+}$  has been performed with the AMBiT code [10]. Our calculation begins with a Dirac-Hartree-Fock calculation of Ne-like Fe to construct the core  $1s$ ,  $2s$ , and  $2p$  orbitals in the  $V^N$  potential. The Breit interaction is included throughout the calculation. We diagonalize a set of  $B$ -splines in the Dirac-Fock potential to obtain valence orbitals. Configuration interaction is performed using the particle-hole CI method [11], however, this can be mapped exactly to the electron-only approach described in Section II A.

Our basic calculation is presented on the first line of Table VI. The CI space consists of all possible single and double excitations up to  $10spdf$  from the same set of leading configurations presented previously:  $2s^2 2p^6, 2p^{-1} 3p, 2p^{-1} 3s, 2p^{-1} 3d, 2p^{-1} 4d, 2p^{-1} 5d$ , and  $2s^{-1} 3p$ . At this stage, we do not include excitations from the frozen  $1s^2$  core. Even for this calculation, the matrix size for the odd-parity  $J = 1$  levels is  $N = 479075$ . To reduce the number of stored matrix elements we use emu CI [12], where interactions between high-lying configuration state functions are ignored. We limit the smaller side of the matrix to only including double excitations up to  $5spdf$  and limit the number of  $2s$  and  $2p$  holes to single removals from an expanded set of leading configurations which include, in addition to those listed above,  $2p^{-2} 3d^2, 2p^{-1} 2s^{-1} 3d^2$ , and  $2s^{-2} 3d^2$ . This results in a reduced small side  $N_{\text{small}} = 80497$ . We have checked that expanding the configuration state functions included in  $N_{\text{small}}$  makes no difference to our results at the displayed accuracy.

All of our calculations include the Breit interaction at all stages, and the dipole matrix elements are calculated in the relativistic formulation with  $\omega = 30$  a.u. In the second and third lines of Table VI, we show the effects of removing the Breit interaction and using the static dipole matrix element ( $\omega = 0$ ), respectively.

We then expand our calculation to include  $g$ -wave excitations, up to basis  $10spdfg$ . The difference from  $10spdf$  is shown in the fourth line of Table VI. We see in the AMBiT calculation very little effect from the inclusion of these waves. In the fifth line, we show the effect of allowing excitations from  $1s^2$ , and in the sixth line we see the effect of including the Uehling potential [13] and self-energy [14] using the radiative-potential method [15]. This broadly agrees with the model-operator QED presented in Table IV.

The final row of Table VI gives the results including excitations to  $g$ -waves, excitations from  $1s^2$ , and QED effects. The total number of configuration state functions accounted for is over 1.25 million for the odd-parity  $J = 1$  symmetry. Nevertheless, the CI is not quite converged with respect to including orbitals with  $n > 10$ . We estimate based on calculations for  $8spdf$  and  $12spdf$  that the uncertainty in level energies is conservatively of order  $3000 \text{ cm}^{-1}$  and for the ratio  $gf_{3C}/gf_{3D}$  is of order 0.05. These results are consistent with the CI calculation presented in Sec. II A and the MCDHF results presented in Sec. II B.

TABLE VI. Particle-hole CI calculations using AMBiT of the level energies  $E_{3C}$  and  $E_{3D}$  ( $\text{cm}^{-1}$ ), reduced matrix elements  $D(3C)$  and  $D(3D)$  (a.u.), and ratio of oscillator strengths of the  $3C$  and  $3D$  transitions in  $\text{Fe}^{16+}$ .

	$E_{3C}$	$E_{3D}$	$D(3C)$	$D(3D)$	$gf_{3C}/gf_{3D}$
[10spd $f$ ]	6661400	6552424	0.33893	0.17992	3.607
without Breit	6668847	6557636	0.33758	0.18164	3.511
$\omega = 0$			0.33937	0.18009	3.610
+ [10g]	-15	-13	-0.000001	0.000003	
+ $1s^2$	-103	-85	-0.000040	0.000016	
+ QED	235	94	-0.00012	0.00031	
Final	6661517	6552420	0.33877	0.18025	3.591

---

[1] S. Bernitt, G. V. Brown, J. K. Rudolph, R. Steinbrugge, A. Graf, M. Leutenegger, S. W. Epp, S. Eberle, K. Kubicek, V. Mackel, M. C. Simon, E. Trabert, E. W. Magee, C. Beilmann, N. Hell, S. Schippers, A. Muller, S. M. Kahn, A. Surzhykov, Z. Harman, C. H. Keitel, J. Clementson, F. S. Porter, W. Schlotter, J. J. Turner, J. Ullrich, P. Beiersdorfer, and J. R. C. López-Urrutia, *Nature* **492**, 225 (2012).

[2] C. R. Canizares, D. P. Huenemoerder, D. S. Davis, D. Dewey, K. A. Flanagan, J. Houck, T. H. Markert, H. L. Marshall, M. L. Schattenburg, N. S. Schulz, M. Wise, J. J. Drake, and N. S. Brickhouse, *Astrophys. J. Lett.* **539**, L41 (2000).

[3] C. Wu and X. Gao, *Sci. Rep.* **9**, 7463 (2019).

[4] I. I. Tupitsyn, M. G. Kozlov, M. S. Safronova, V. M. Shabaev, and V. A. Dzuba, *Phys. Rev. Lett.* **117**, 253001 (2016).

[5] V. A. Dzuba, V. V. Flambaum, and M. G. Kozlov, *Phys. Rev. A* **54**, 3948 (1996).

[6] A. Kramida, Yu. Ralchenko, J. Reader, and and NIST ASD Team, NIST Atomic Spectra Database (ver. 5.6.1), [Online]. Available: <https://physics.nist.gov/asd> [2019, September 6]. National Institute of Standards and Technology, Gaithersburg, MD. (2018).

[7] A. Kramida, Preliminary critical analysis of Fe XVII spectral data, Private Communication (2019).

[8] C. F. Fischer, G. Gaigalas, P. Jónasson, and J. BieroÅ, *Comput. Phys. Commun.* **237**, 184 (2019).

[9] P. Jónasson, P. Bengtsson, J. Ekman, S. Gustafsson, L. Karlsson, G. Gaigalas, C. F. Fischer, D. Kato, I. Murakami, H. Sakaue, H. Hara, T. Watanabe, N. Nakamura, and N. Yamamoto, *At. Data Nucl. Data Tables* **100**, 1 (2014).

[10] E. V. Kahl and J. C. Berengut, *Comput. Phys. Commun.* **238**, 232 (2019).

[11] J. C. Berengut, *Phys. Rev. A* **94**, 012502 (2016).

[12] A. J. Geddes, D. A. Czapski, E. V. Kahl, and J. C. Berengut, *Phys. Rev. A* **98**, 042508 (2018).

[13] J. S. M. Ginges and J. C. Berengut, *J. Phys. B: At., Mol. Opt. Phys.* **49**, 095001 (2016).

[14] J. S. M. Ginges and J. C. Berengut, *Phys. Rev. A* **93**, 052509 (2016).

[15] V. V. Flambaum and J. S. M. Ginges, *Phys. Rev. A* **72**, 052115 (2005).